Influence of the time-dependent pulse spectrum on ionization and laser propagation in nonlinear optical materials

Guillaume Duchateau[1,*] and Antoine Bourgeade[2,*]

[1]*Université de Bordeaux, Centre National de la Recherche Scientifique, Commissariat à l'Énergie Atomique et aux Énergies Alternatives, Centre Lasers Intenses et Applications, Unités Mixtes de Recherche 5107, 351 Cours de la Libération, 33405 Talence Cedex, France*

[2]*Commissariat à l'Énergie Atomique et aux Énergies Alternatives, Centre d'Etudes Scientifiques et Techniques d'Aquitaine, BP2, 33114 Le Barp, France*

(Received 19 March 2014; published 28 May 2014)

The interaction and the propagation of intense and short laser pulses in nonlinear optical materials are addressed. A consistent introduction of a time-dependent ionization model into the Maxwell's equations allows one to account for the influence of strong variations of the pulse spectrum on the ionization dynamics, which in turn affects the pulse propagation. The interaction between both ionization and propagation dynamics is demonstrated for two cases of practical interest: frequency conversion and propagation of chirped pulses.

DOI: 10.1103/PhysRevA.89.053837 PACS number(s): 42.25.Bs, 52.50.Jm, 79.20.Ws

I. INTRODUCTION

Optical materials, such as silica, Sb_2O_3 (BK7), LiB_3O_5 (LBO), BaB_2O_4 (BBO), KH_2PO_4 (KDP), $KTiOPO_4$ (KTP), soda limes, or sapphire, are commonly used in laser systems for pulse shaping. These materials are dielectrics with large band gaps, and their electronic properties may significantly evolve when interacting with intense femtosecond laser pulses [1,2]. At the same time, laser-pulse characteristics such as the intensity profile of the frequency spectrum may be strongly affected in the course of propagation [3,4]. The modifications of electronic properties begin at the ionization stage due to either multiphoton absorption (MPA) or tunneling. The electron transition from the valence band (VB) to the conduction band (CB) is followed by various processes including heating in the CB, impact ionization, and various kinds of electron collisions [5,6]. Since most of these processes depend on the electron density in the CB, an accurate description of the primary ionization stage is required. This is all the more important for the nonlinear processes that are modifying the frequency spectrum, such as frequency conversion, frequency drift, or spectral broadening. In particular, the ionization dynamics may be strongly affected by a change in the multiphoton order due to significant variations of the frequency spectrum in the course of propagation [7,8]. Because of the intrinsic relation between ionization and absorption, instantaneous changes in the rate of production of conduction electrons may in turn affect the propagation dynamics of the laser pulse [3,9].

An accurate description of the above-mentioned physical phenomena thus can be only achieved by modeling laser-pulse propagation together with an accurate description of the primary ionization, which accounts for possible variations of laser-pulse characteristics including time-dependent frequency spectra and associated MPA orders. A time-dependent description of the ionization stage is thus required [4,7,8], which cannot be correctly described by a stationary approach such as the well-known Keldysh model [10,11]. Indeed, it assumes that the laser frequency is explicitly known, i.e., a perfect monochromatic wave is assumed whereas such conditions are not fulfilled generally. More precisely, a time-dependent model including explicitly the temporal variations of the laser electric field is required. Such a model carries implicitly all information about the frequency spectrum (through Fourier transform) and thus accounts for possible simultaneous MPA orders due to the pulse spectral width.

Abandoning the assumption of a fixed monochromatic wave, we will be working within the time domain. The best way to describe the propagation of short laser pulses in dielectric materials under these conditions is to solve numerically the three-dimensional (3D) Maxwell equations (numerical code solving of Maxwell's equations is hereafter referred to as CME), which can also serve to validate less general models. In the present work, this is achieved by using a 3D finite-difference time domain (FDTD) scheme [12–14]. Note that other approaches based on the resolution of the so-called nonlinear Schrödinger equation (NLSE) or the unidirectional pulse propagation equation would also be appropriate [3,15]. A good candidate for modeling the primary ionization stage is the so-called BVkP approach, which is based on Bloch-Volkov states describing the quantum dynamics of an electron in both the lattice and laser electric fields [9]. It has been shown to correctly account for the possible temporal evolution of the frequency spectrum through the time-dependent electric field, thus being able to describe consistently the simultaneous presence of various MPA orders due to spectral broadening or temporal evolution due to a frequency chirp [9]. The moderate laser intensities considered in this work prevent us from significant tunnel ionization as a primary ionization process, which is thus not considered hereafter. The aim of the present paper is to couple both CME and BVkP approaches to account consistently of various time-dependent ionization paths in the course of propagation and to exhibit the physical consequences resulting from this consistent description. After reviewing briefly both the propagation and ionization models, the coupling method is presented. The influence of the introduction of a time-dependent ionization model in a propagation code is studied with three cases of practical interest: frequency conversion in both KDP crystal and silica and propagation of a chirped pulse in silica [16]. The results show significant effects of this consistent description of time-dependent laser-matter interaction on the temporal pulse-shape evolution and ionized

*duchateau@celia.u-bordeaux1.fr; antoine.bourgeade@cea.fr

material area along the propagation axis. It is worth noting that the present work does not address a full description of all involved physical processes. The main goal of this work is to demonstrate the reliability of the present approach and to address the main physical consequences of a consistent coupling of ionization and pulse propagation. To do so, in order to enhance the consequences of accounting for pulse spectrum, the studied cases have been slightly simplified by removing a physical effect which is only expected to introduce a less important ionization-propagation coupling in real conditions.

II. THEORY

The model includes the laser-pulse propagation module coupled consistently with the multiphoton ionization (MPI) module as follows. The propagation of the laser pulse is based on a 3D FDTD scheme as developed initially by Yee [17]. By means of leapfrog and centered finite-difference techniques, this approach provides a numerical scheme which is of the second order in both space and time. A parallel version of such a code has been developed, allowing us to perform calculations efficiently [12]. Such an approach keeps track of every frequency and allows us to compute all three spatial components of the fields, including also possibly the component of the electric field in the direction of propagation.

The time-dependent ionization model, called BVkP, is described in [9]. Hereafter are summarized the main particularities of this approach, where atomic units are used unless otherwise stated. Under the assumptions of the electric dipole approximation and the single-active electron, it is based on an evaluation of the quantum transition amplitude from the initial unperturbed valence state $\varphi_v(\vec{r},t)$ to the final perturbed conduction state $\Psi_c(\vec{r},t)$ within the length gauge:

$$T_{cv}(t) = -i \int_0^t dt \langle \Psi_c(t) | \vec{r} \cdot \vec{E}(t) | \varphi_v(t) \rangle, \tag{1}$$

with $\Psi_c(\vec{r},t)$ describing an electron in both the laser electric field $\vec{E}(t)$ and the crystalline field, which can be approximated by a Bloch-Volkov state $\chi_c^{\mathrm{BV}}(\vec{r},t)$ [18]:

$$\begin{aligned}\Psi_c(\vec{r},t) &\simeq \chi_c^{\mathrm{BV}}(\vec{r},t) \\ &= \varphi_c(t) \times \exp\left\{ i\vec{A}(t)\cdot\vec{r} - i\int_0^t dt' \frac{[A(t')]^2}{2m_c} \right\}, \end{aligned} \tag{2}$$

with $\varphi_c(\vec{r},t)$ the unperturbed conduction state, $\vec{A}(t)$ the vector potential such that $\vec{E}(t) = -\partial\vec{A}(t)/\partial t$, and m_c the electron mass in the conduction band. The exponential term in Eq. (2) is the so-called Volkov phase. After some analytics and using the $\vec{k}\cdot\hat{P}$ theory to evaluate the matrix elements [9,19], the transition amplitude takes the following simple expression:

$$\begin{aligned} T_{cv}(t) = &-\frac{P}{m_0(E_c - E_v)} \\ &\times \int_0^t dt \exp\{i(E_c - E_v)t\} \frac{E(t)}{[1 - iA(t)/\alpha]^2}, \end{aligned} \tag{3}$$

with $E_c - E_v$ the energy gap between valence and conduction states and α the only parameter of the present model which is related to the spatial expansion of the valence wave function, set to 1.55 a.u. as in [9], allowing us to retrieve MPI cross sections similar to Keldysh predictions for relatively long pulses. The prefactor P is related to the matrix element and evaluated through the $\vec{k}\cdot\hat{P}$ theory:

$$P = \langle \phi_c | \hat{P}_Z | \phi_v \rangle = \sqrt{\frac{m_0^2 E_g}{2m_{vc}^*}} \quad \text{with} \quad \frac{1}{m_{vc}^*} = \frac{1}{m_v^*} + \frac{1}{m_c^*}, \tag{4}$$

where $\vec{P} = -i\vec{\nabla}$ is the momentum operator; E_g is the band gap; and m_0, m_v, and m_{vc} are the electron masses in the free space, the valence band, and the reduced particle. Finally, from the expression of the transition amplitude, the ionization rate which has to be introduced in the appropriated term of the Maxwell equations reads

$$\begin{aligned} W_{\mathrm{MPI}}(t) = \frac{\partial n_e}{\partial t} &= N_0 \sum_c \frac{\partial |T_{cv}(t)|^2}{\partial t} \\ &= 2N_0 \sum_c \mathrm{Re}\left\{ T_{cv}^*(t) \frac{\partial T_{cv}(t)}{\partial t} \right\}, \end{aligned} \tag{5}$$

where N_0 is the density of valence electrons, set to 2.2×10^{22} cm^{-3} in the present study, and the sum over various conduction states accounts for a possibly complex CB. Note that, in case of frequency conversion where the harmonic electric field may be perpendicular to the incident electric field, the total ionization rate is obtained by summing the ionization rates corresponding to each crystalline axis.

The as-previously evaluated electron density n_e produced in the conduction band only describes the interaction of an electron with the laser electric field and accounts for the lattice periodicity but does not account for possible collisions with phonons, ions, or other electrons. Due to these collisions, the coherence between the excited electron to the CB and its parent ion is destroyed and may introduce deviations from the above-predicted evolution of the electron density in the CB with respect to time. Indeed, without collisions, the produced electron density was shown to oscillate with time due to the fact that a conduction electron may go back and forth to the VB through the action of the electromagnetic field [9]. We thus defined a free state as a state where the electrons can be heated by inverse bremsstrahlung (IB) and are decorrelated from the parent ions. The density of electrons associated with this free state is called n_{FE}. From a general point of view, the collisions lead the laser produced electrons to relax to the free-electron state with the density n_{FE} with a characteristic time τ_d. This time may also be seen as a decoherence time associated with phonon characteristic time. Since these free electrons are produced, they can be heated through IB and lead to impact ionization with an efficiency η, and also recombine with a characteristic time τ_r. The electron heating is described with a standard Drude model, which provides the expression of η where the collision frequency depends on temperature as in [20]. The evolution of the free-electron density can then be simply described by the following rate equation:

$$\frac{dn_{\mathrm{FE}}}{dt} = \frac{n_e}{\tau_d} + \eta n_{\mathrm{FE}} - \frac{n_{\mathrm{FE}}}{\tau_r}. \tag{6}$$

Based on experimental data [21–23] and modeling results [9], the value of the relaxation time lies in the picosecond range and is set to 3 ps in the present work. τ_r is set to 150 fs, which is a

correct order of magnitude for silica and KDP crystals [21,24]. Finally, the depletion of the initial valence state is introduced in order to keep the total electron density constant. It is worth noting that we have checked that physically reasonable variations of the previously set parameters $(N_0,\alpha,\tau_d,\tau_r)$ lead to similar physical trends as those presented hereafter.

The coupling between the BVkP ionization rate and the CME is made through a fictive ionization current $\vec{J}_i$ due to the produced electrons with rate n_e/τ_d, which accounts for the laser absorbed energy required to promote the valence electron to the CB through MPA. The modified Maxwell equation accounting for this influence reads [20,25]

$$\frac{\partial \vec{D}}{\partial t} = \vec{\nabla} \times \vec{H} + \vec{J}_e + \vec{J}_i, \tag{7}$$

with $\vec{D}$ and $\vec{H}$ the electric displacement and the magnetic induction, respectively. $\vec{J}_e$ is the conduction current associated with the displacement of free electrons, accounting in particular for the Joule effect. The latter is modeled through a Drude model depending on the free-electron density n_{FE} and the collision frequency as previously described. The ionization current $\vec{J}_i$ accounts for energy transfer due to the MPA, according to the energy balance equation:

$$\frac{\partial W}{\partial t} = \vec{E} \cdot \vec{J}_i = -\frac{n_e}{\tau_d} W_i, \tag{8}$$

where W is the laser energy density and W_i is the energy required to promote a valence electron to the CB, i.e., the band gap. This leads to the following definition of $\vec{J}_i$ [assuming that $E(t)$ is different from zero]:

$$\vec{J}_i(t) = -W_i \frac{n_e}{\tau_d} \frac{\vec{E}(t)}{E(t)^2}. \tag{9}$$

In the case of a phenomenological law for the ionization rate proportional to E^{2n}, Eq. (9) leads to a finite value of $\vec{J}_i$ even for arbitrary small values of $E(t)$ since the denominator in E of Eq. (9) cancels, leading to $J_i \propto E^{2n-1}$. Within the BVkP approach, the ionization rate is no longer proportional to E^{2n} but also depends on the vector potential, accounting for possible retardation effects during the ionization process. It then turns out that $\vec{J}_i$ diverges for $E(t)$ tending to zero. This is an unphysical behavior due to the way $\vec{J}_i(t)$ is constructed, which may lead to numerical instabilities. It is noteworthy that no more reliable coupling formulation was proposed to our knowledge. To overcome this problem, the relaxation time in the present model is related to the electric field as $\tau_d \propto E^{-1}$ if the latter becomes too small, i.e., smaller than 20 times the maximum of the electric field in practice. This choice allows us to avoid the unphysical divergence. It can be supported by physical considerations related to the classical dynamics of a particle subjected to an electric field and the friction force. Since the classical relation $mdv/dt + mv/\tau_d = -eE$ leads to the stationary solution, $v = -eE\tau_d/m$ and thus $\tau_d \propto E^{-1}$. Despite the fact that the latter relation has been established with empirical considerations, it provides a physical meaning and makes the present coupling more consistent. This approach has been confirmed to remove instabilities and not to induce spurious behaviors. Finally, the evaluation of the BVkP ionization rate requires the evaluation of the vector potential, which is simply done by numerically integrating the electric field provided by the CME.

We have checked that the influence of impact ionization on the production of free electrons is negligible compared to the MPI under the present laser conditions unless otherwise stated. In particular, electron avalanche does not take place. This physical process is thus no longer discussed in the following.

III. RESULTS AND DISCUSSION

The previous ionization-propagation model is applied for description of the propagation of an intense fs laser pulse in a potassium dihydrogen phosphate crystal (KH_2PO_4 or KDP). Since this optical material is a frequency converter, the number of photons required to ionize may vary in the course of propagation. This case is thus well suited to show the ability of the present approach to account for various ionization paths depending on the propagation distance. The simulation is performed with the following parameters for the laser pulse: initial wavelength $\lambda = 633$ nm, pulse length (full width at half maximum) of $\tau = 80$ fs with a Gaussian envelope, and a maximum electric field of 6×10^9 V/m corresponding to a maximum intensity of $\sim$7.5 TW/cm^2. Regarding the material properties, they are modeled with a band gap of 7.8 eV [24] and a realistic second-order susceptibility of $\chi^{(2)} = 4.35 \times 10^{-13}$ m/V [12]. With these physical parameters, four fundamental photons are required to promote valence electrons to the CB, whereas only two are required with the second-harmonic radiation (2ω).

Under these conditions, Fig. 1 shows the evolution of the pulse energy density for both the fundamental and the second-harmonic radiation as a function of the propagation distance in various cases. In order to evaluate the influence of ionization, results with no ionization included are first reported (black curves). In that case, as expected, the energy density of the fundamental radiation decreases whereas the harmonic one increases, the sum of both being constant in the course of propagation accounting for the energy conservation.

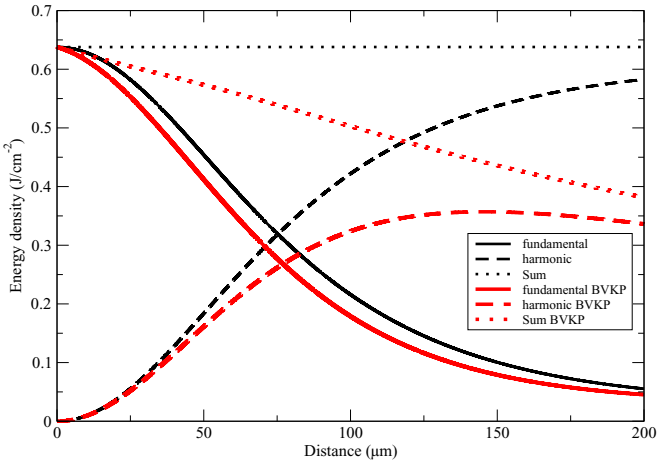

FIG. 1. (Color online) In the case of laser-pulse propagation in a frequency converter KDP crystal, evolution of the energy density of the fundamental laser pulse and its second harmonic as a function of the propagation distance. Calculations without and with ionization (with the BVkP approach) are presented.

When ionization is included through the BVkP model, the evolution of the harmonic pulse is significantly different (red curves). Indeed, since only two photons of the 2ω radiation are required to bridge the band gap, the ionization rate is large, thus leading to significant absorption of the harmonic pulse by valence electrons and subsequent heating by IB. Regarding the fundamental pulse, the influence of ionization on its energy density is not significant due to a relatively high MPI order ($n = 4$). It mainly occurs at the beginning of the propagation, where the fundamental intensity is the largest. Note that laser energy depletion due to IB and ionization are equivalent under the present conditions. Finally, the decrease in the total laser energy corresponds to the energy transfer into the electron system (red dashed curve).

The previous considerations are confirmed by Fig. 2(a), which shows the evolution of the maximum of the free-electron density as a function of the propagation distance in two cases. First, when the frequency conversion is not allowed [$\chi^{(2)}$ is set to zero in the CME], the black curve shows an exponential decrease in the electron density associated with the depletion of the laser pulse. This behavior corresponds to the standard Beer-Lambert law ($dI/dz = -\alpha I^n - \beta I$, where

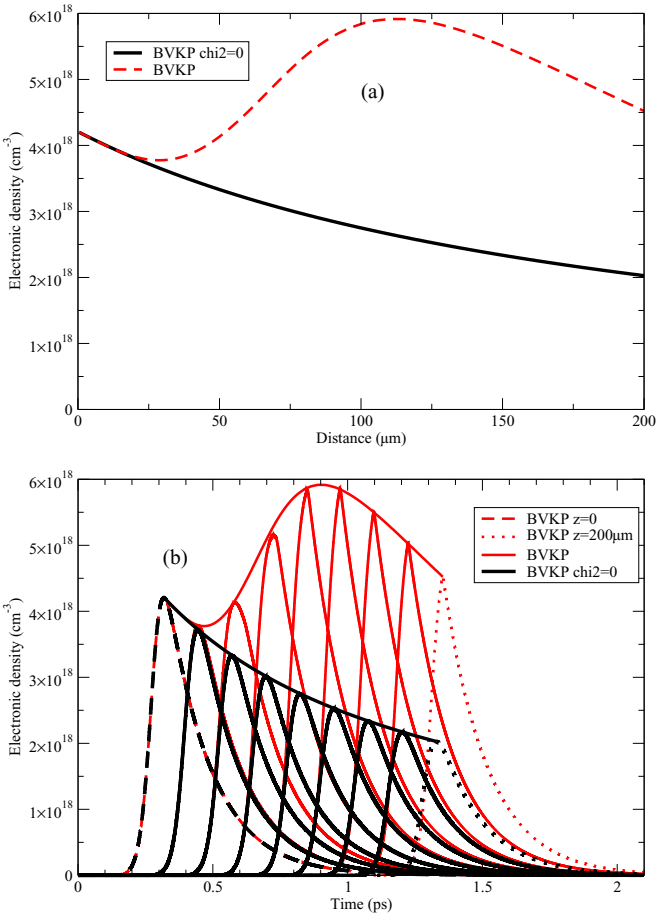

FIG. 2. (Color online) (a) Evolution of the maximum free-electron density n_{FE} as a function of the propagation distance without (black curve) and with (red curve) frequency conversion in KDP crystals. (b) Temporal evolution of the free-electron density for various propagation distances from 0 to 200 μm. The evolution of the maximum of the electron density is shown.

the first term in the right-hand side accounts for the pulse absorption due to MPI and the second term accounts for IB). Second, when frequency conversion is allowed (red curve), this behavior is dramatically changed due the additional ionization path created by the second-harmonic generation. When the latter becomes significant, roughly after a few tens of μm of propagation, the two-photon ionization rate is such that it compensates absorption due to the initial four-photon ionization decreasing, even leading to an increase in the free-electron density with respect to the propagation distance as the harmonic intensity is increasing. After roughly 100 μm of propagation, the generation of the second harmonic and its absorption equilibrate, leading to the maximum of induced CB electron density. After this point, harmonic generation is no longer efficient due to the pump depletion. The harmonic signal is then mainly absorbed due to MPI and IB during its propagation, again leading to a decrease in its energy density with a Beer-Lambert behavior, which subsequently leads to a decrease in the produced CB electron density. These considerations are further supported by Fig. 2(b), which shows the temporal evolution of the CB electron density for various propagation distance from 0 to 200 μm. For a given distance, this figure first illustrates how the maximum density is extracted with respect to the temporal evolution. The associated envelope corresponding to the evolution of the maximum in the course of propagation exhibits a very similar shape as the one of Fig. 2(a), thus confirming the previous analysis and indicating that the group velocity of the laser pulse is mainly constant. For a given distance, profiles of Fig. 2(b) also indicate the presence of asymmetry in the temporal evolution of the CB electron density: first, free electrons are quickly produced (left side of a given profile) due to the rise in the laser intensity. When the laser intensity drops, the decrease in the electron density takes place on a longer timescale accounting for intrinsic relaxation processes no longer related to the laser-pulse variations.

Hereafter is presented a study of the nonlinear propagation of an intense laser pulse in fused silica. The dispersion effect has been switched off in order to enhance the production of harmonic pulses (coherent emission of harmonic radiation) and thus to enhance the coupling between nonlinear ionization and propagation. Despite the fact that physical influence of dispersion is missing, this case has been chosen to strengthen the previous conclusion regarding frequency conversion. As shown hereafter, this case also clearly exhibits the reliability of the present time-dependent treatment of MPI during propagation. Here, the third-order nonlinearities are expected instead of the second-order ones of the previous example. This case is studied with the following characteristics for the laser pulse: initial wavelength $\lambda = 400$ nm, temporal characteristics similar to the previous case, and a maximum electric field of 2×10^9 V/m corresponding to an intensity of $\sim$0.83 TW/cm^2. Regarding the material properties, they are modeled with a band gap of 9 eV and a realistic third-order susceptibility $\chi^{(3)} = 2 \times 10^{-22}$ m^2/V^2 [26] (since fused silica is a centrosymmetric material the second-order susceptibility is zero). With these physical parameters, three fundamental photons are required to promote valence electrons to the conduction band, whereas only one is required for the third-harmonic radiation.

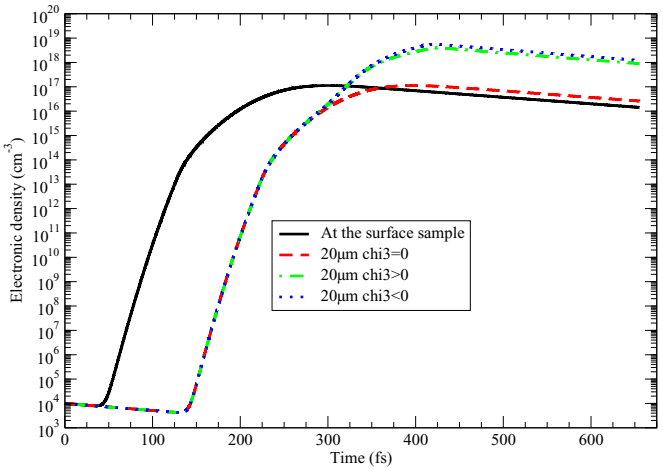

FIG. 3. (Color online) For frequency conversion in silica, evolution of the free-electron density n_{FE} as a function of time at the surface and after 20 μm of propagation in three cases: $\chi^{(3)} = 0$, $\chi^{(3)} > 0$, and $\chi^{(3)} < 0$.

Figure 3 presents the temporal evolution of the free-electron density after 20 μm of propagation for three cases: $\chi^{(3)} = 0$, $\chi^{(3)} > 0$, and $\chi^{(3)} < 0$, where the absolute value of the susceptibility is the one provided before. These results can be compared to the reference case of the electron density at the surface with no propagation effect. The density shapes at the surface or after propagation of 20 μm with $\chi^{(3)} = 0$ are very similar, indicating no significant modification of the laser pulse during propagation: no absorption, since the initial intensity is too low, and no frequency conversion, since $\chi^{(3)} = 0$. This shape consists of a fast increase up to roughly the maximum of the laser electric field, followed by a slow decrease accounting for recombination to the VB. When $\chi^{(3)}$ is different from zero, the maximum electron density is increased by a factor of ~50. With respect to time, the departure of this electron density from the one obtained with $\chi^{(3)} = 0$ takes place near the maximum of the electric field, suggesting the expected presence of nonlinear effects. This departure is due to third-harmonic generation (THG) as depicted by Fig. 4, which shows the spectral components of the laser electric field at 1ω and 3ω. Instead of a three-photon MPI process induced by the fundamental pulse, a one-photon process is allowed by the third harmonic, thus leading to a strong increase in the ionization rate in the course of propagation as long as the amplitude of the third harmonic is increasing.

Figure 4(a) shows the frequency spectrum of the laser electric field around the fundamental radiation after a propagation over 20 μm, obtained through a Fourier transform in various cases: with or without ionization and with various signs of $\chi^{(3)}$. Without ionization and whatever the value of $\chi^{(3)}$, or with ionization and $\chi^{(3)} = 0$, the spectra exhibit the same shape above 1×10^{11} a.u., accounting for the fact that there is no perturbation due to nonlinear effects under these conditions. When ionization is allowed and $\chi^{(3)}$ is different from zero, spectral broadening takes place, accounting for the electron contribution to the susceptibility. This is confirmed by Fig. 4(b), which shows the frequency spectrum around the third harmonic within the same configurations as in Fig. 4(a):

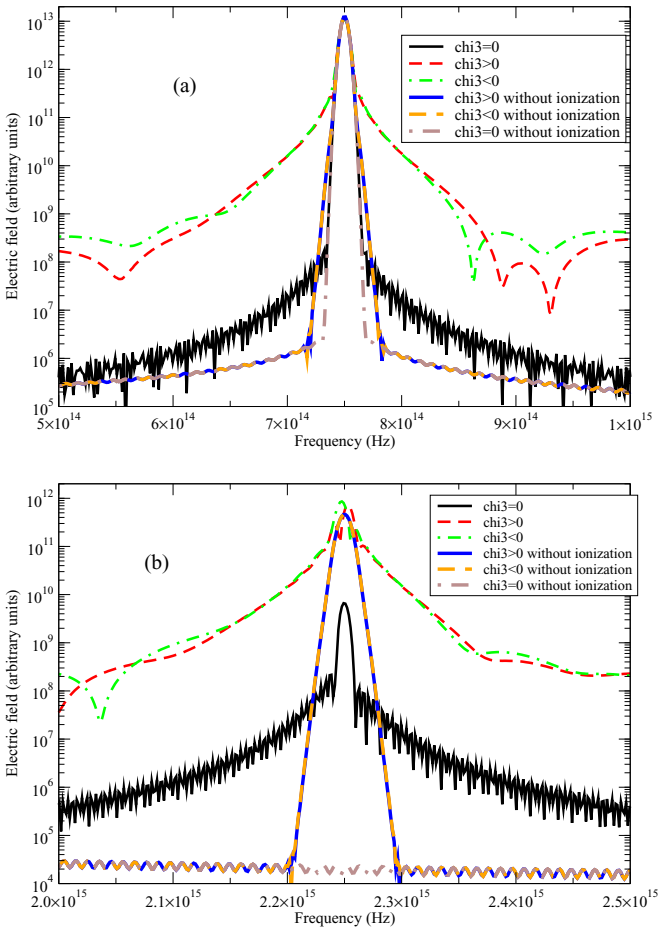

FIG. 4. (Color online) (a) Spectra of the fundamental laser pulse in various cases after a propagation of 20 μm in silica where third-harmonic generation takes place. (b) Same as previously for the third harmonic.

when $\chi^{(3)} = 0$, no significant third-harmonic generation takes place. As expected, since $\chi^{(3)}$ is different from zero, significant THG occurs. When ionization is introduced, first THG is more efficient, further indicating the contribution of CB electrons to $\chi^{(3)}$. Indeed, a Fourier transform of $n_{FE}(t)$ shows a significant component at 2ω (due to the fact that ionization mainly takes place every half optical cycle). The combination of both the fundamental radiation at ω and the previous 2ω contribution in the Maxwell equations then can lead to the observed additional THG. Furthermore, discrepancies between $\chi^{(3)} > 0$ and $\chi^{(3)} < 0$ can be observed. First, in both cases, a slight shift in the central frequency appears, the sign of which depends on the one of $\chi^{(3)}$. Second, $\chi^{(3)} < 0$ leads to a better THG than the $\chi^{(3)} > 0$ configuration. The influence of these slight differences appearing in the THG is correctly taken into account by the BVkP model, which predicts discrepancies in the free-electron production depending on the sign of $\chi^{(3)}$ as shown by Fig. 3.

Now, the case of a chirped pulse propagating in fused silica is considered. This case is studied with the following parameters for the laser pulse: initial central wavelength $\lambda = 333$ nm (3.54 eV) with a spectral broadening of roughly 4×10^{14} Hz (0.7 eV) at 10% of the maximum intensity.

Temporal pulse characteristics are similar to the previous case, and a maximum electric field of 4×10^{10} V/m corresponding to a maximum intensity of roughly 330 TW/cm^2 has been chosen. Regarding the material properties, they are modeled with a band gap of 9 eV. Contrary to the previous case, time dispersion is reintroduced to allow various frequencies to propagate at different speeds, but $\chi^{(3)}$ is set to zero in order to only exhibit the influence of the chirp on both coupled ionization and pulse propagation. Doing so, we can separate such physical effects as chirp and frequency conversion, thus exhibiting clearly the influences of each process. Within the present conditions, ionization takes place first with a three-photon absorption followed by a four-photon absorption or the opposite depending on the chirp sign.

In order to exhibit the influence of instantaneous frequency variations, the BVkP approach is compared to a simple model, called EIM for empirical ionization model, accounting for multiphoton absorption only through a generalized cross section, i.e., defining the ionization rate as $W = \sigma_n I^n N_0$ where n is the number of simultaneously absorbed photons to bridge the band gap. Under the present conditions, n is set to 3, which corresponds to the central wavelength of the presently used chirped pulse, and σ_3 has been set to 10^{-55} m^6 s^2 J^{-3} in order to estimate an order of magnitude for ionization comparable to the BVkP prediction. We emphasize that the EIM model does not account for frequency variations within the laser pulse.

Figure 5 shows the evolution of the free-electron density in the CB as a function of time at $z = 0$ as predicted by both the BVkP approach and EIM model, and with both positive (increasing frequency) and negative (decreasing frequency) chirps. As expected, the EIM approach provides similar density evolutions whatever the sign of the chirp since no time-dependent frequency is included in this model: the evolution of the free-electron density consists of a rapid increase up to the maximum allowed value (full depletion of the valence band due to impact ionization) followed by a decrease related to recombinations. For a negative chirp, the BVkP approach predicts the same trends because the interaction also begins with the three-photon absorption. When the four-photon absorption takes place, the density is already saturated, thus leading to similar predictions as the EIM approach. However, the density as predicted by the BVkP approach begins to decrease before the EIM prediction because the four-photon rate is not sufficient to sustain the density at the saturated value during the same temporal interval as the EIM model predicts a larger ionization rate. For a positive chirp, the BVkP predicts a slower increase in the density, thus accounting correctly for the fact that the interaction begins with a four-photon absorption whose associated ionization rate is slower than the three-photon one. This case thus confirms the ability of the BVkP approach to account for time-dependent variations of pulse characteristics.

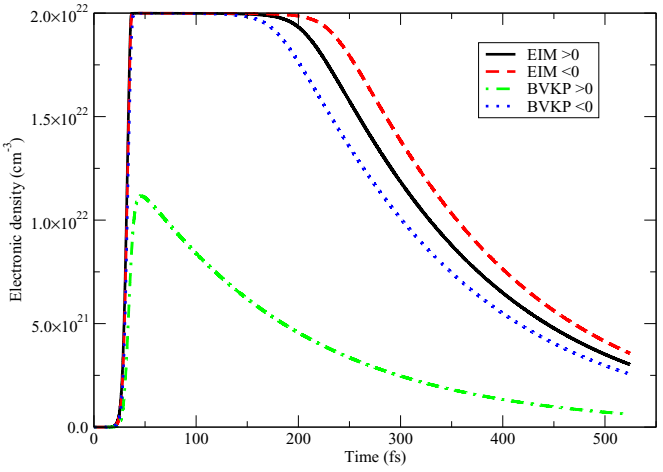

FIG. 5. (Color online) Evolution of the free-electron density n_{FE} as a function of time at $z = 0$ (without propagation) as predicted by both EIM and BVkP approaches for a laser pulse in silica with both positive and negative chirps.

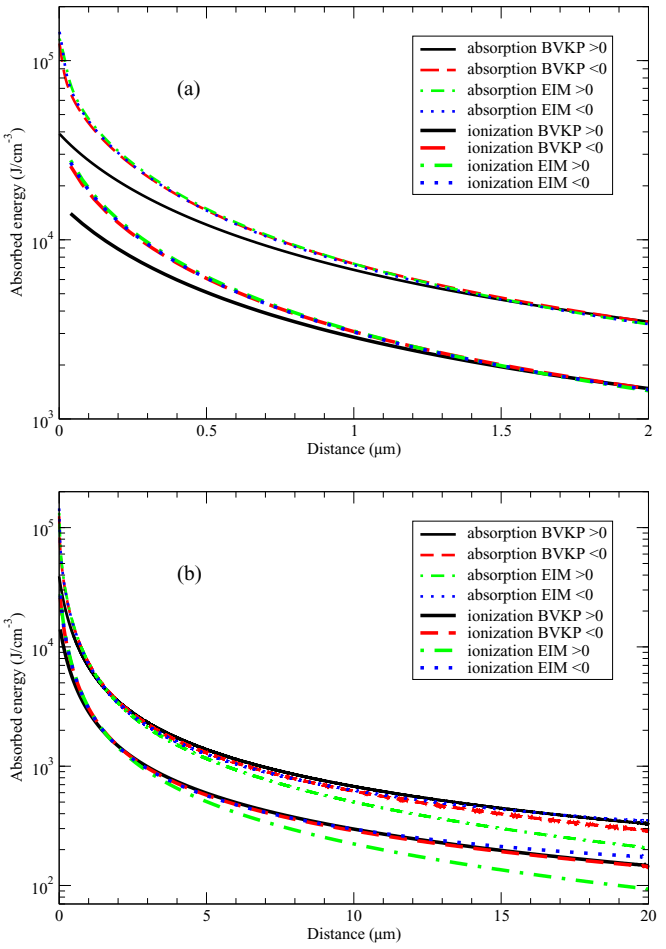

FIG. 6. (Color online) Evolution of the absorbed energy density to ionize (dashed lines) and to both ionize and heat by inverse bremsstrahlung (solid lines) as a function of the propagation distance in silica with chirped pulses as predicted by both EIM and BVkP approaches. (a) Focus on a relatively short propagation distance from 0 to 2 μm. (b) Propagation over longer distances up to 20 μm.

The observations related to the density variation in Fig. 5 are confirmed by considering the absorbed energy spent for ionization in Fig. 6(a), which shows its evolution as a function of the propagation distance from 0 to 2 μm. At the origin, the energy spent for ionization is the same for the EIM approach whatever the chirp sign and for the BVkP model with the negative chirp, whereas it is smaller as predicted

by the BVkP approach in the case of positive chirp (dashed lines). The solid lines depict the total laser-pulse absorption due to both ionization and heating of produced conduction electrons. As in the previous case, where only ionization was considered, the BVkP approach with positive chirp always departs from the three others. It turns out that the signature of the chirp sign survives even in the case where all absorption mechanisms are included, whereas the efficiency of heating through IB exhibits an opposite dependence with respect to the laser frequency compared to ionization: the smaller the frequency, the higher the IB heating rate. After a short propagation distance of 2 μm, the chirp sign does not change yet both the ionization and total absorptions, even as predicted by the BVkP approach. This trend then remains unchanged along the propagation up to $z = 20$ μm as shown by Fig. 6(b). This observation can be explained by the fact that the total energy of the positively chirped pulse with BVkP decreases slower than other configurations with the propagation distance, thus leading to a stronger absorption. This slight change is also due to the temporal evolution of the pulse in the course of propagation. Indeed, due to dispersive effects in the propagation speed, it turns out that low laser frequencies travel faster than high frequencies, resulting in a compression of negatively chirped pulses as illustrated by Fig. 7(a), which shows the temporal evolution of the laser electric field for both chirp signs at $z = 20$ μm. As a consequence, more time is available for electronic transitions and associated absorption for positive chirp in the BVkP ionization model. Finally, at $z = 20$ μm, despite the fact that absorbed energies for ionization are similar for BVkP and for both chirp signs, the total absorbed energy for the positive chirp is the largest because longer wavelengths have more time to heat the free electrons. Indeed, this process takes place at the very beginning of the laser pulse, where most of the free electrons have already been produced.

The previous results have shown that the total absorbed energy is mainly due to the free-electron heating by IB. This is confirmed by the frequency spectra of the laser pulse after 20 μm of propagation in the various cases as depicted by Fig. 7(b). A significant heating leading to a decrease in the intensity is possible when the density of free electrons is sufficiently high. In the case of a negative chirp, a significant electron density is produced at the beginning of the pulse, allowing the tail of the pulse, i.e., longest wavelengths, to heat and to induce the largest absorption. This leads to a depopulating of the smallest frequencies. For a positive chirp, a significant density is produced later; the heating thus mainly takes place with the shortest wavelengths. The spectrum thus is depopulated in the high-frequency region. The latter influences are enhanced when modeling the ionization with the BVkP approach since the temporal ionization dynamics is described more accurately than the EIM approach.

Finally, it is worth noting that in the present cases of frequency conversion a coupled set of NLSEs for each frequency as developed in, e.g., [27], associated with the EIM model for ionization, would also be able to provide similar results under conditions where no mixing of both frequencies contributes to the ionization. In the case of a chirped pulse, it could be possible to change the value of n with time in the EIM approach to account for temporal frequency variations. This is possible in this particular case due to the simple evolution of the frequency, thus allowing the establishment of a pertinent criterion for the MPI order. The strength of the present BVkP approach, where a full consideration of the temporal variations of the electric field is included, is to consistently account for the broad spectrum influence on the ionization dynamics in every situation as long as the MPI prevails.

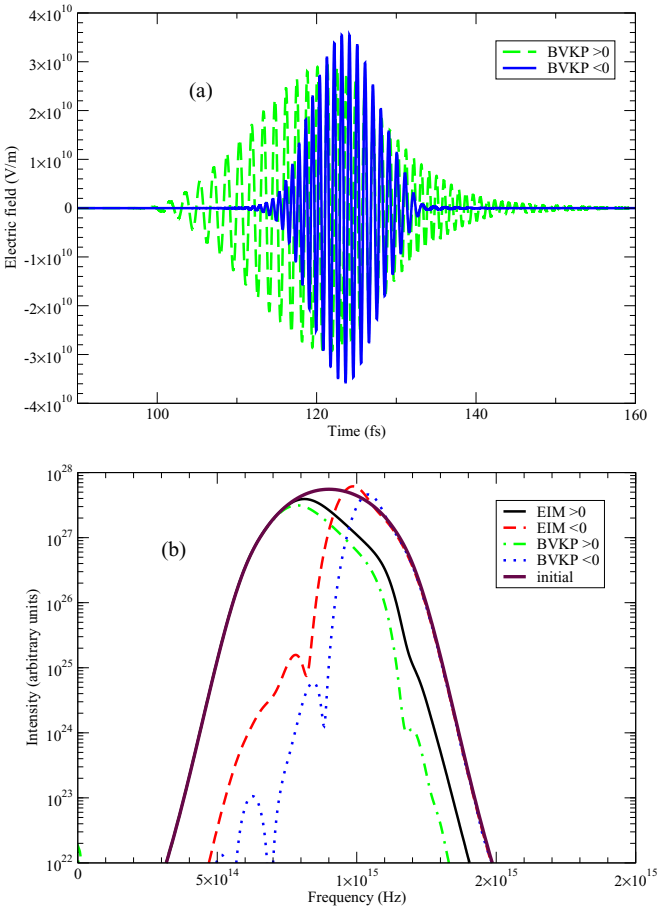

FIG. 7. (Color online) After a propagation over 20 μm in silica of both positively and negatively chirped pulses, (a) evolution of the laser electric field as a function of time and (b) spectra of the laser intensity as predicted by both the EIM and BVkP approaches.

IV. CONCLUSION

To summarize, a time-dependent ionization model and its coupling to a 3D propagation solver have been presented. The present development has been used to model ionization and propagation of a laser pulse in realistic media where strong variations in the frequency spectrum take place. This introduces strong variations in the ionization dynamics, which in turn affects the pulse propagation dynamics.

The frequency conversion cases demonstrate the ability of the BVkP model to account consistently for the evolution of the laser-pulse spectrum through the formation of additional ionization paths to bridge the band gap in the course of propagation. In the case of third-harmonic generation, despite the fact that the intensity of the harmonic is only 1% of the fundamental radiation, the electron production is dramatically

enhanced by a factor of 50. Furthermore, even the influence of the sign of the third-order nonlinear susceptibility is correctly taken into account in the BVkP model, which predicts differences in the free-electron production depending on this sign. In the case of propagation of a chirped pulse, instantaneous variations of the number of photons depending on the chirp sign are correctly described by the present model, which exhibits significantly different ionization dynamics. Despite the fact that a few simplifications of physical effects have been introduced in the present studied cases in order to enhance the influence of the pulse spectrum, such ionization-propagation coupling effects are expected to play a role in real conditions.

The present observations exhibit the highly nonlinear characteristic of such coupled mechanisms and the importance of an accurate and consistent description of the coupling between both ionization and propagation processes. The ability of the BVkP ionization model to account for these physical effects opens a door for further developments to improve the physical description of the interaction by introducing in particular impact ionization also in a consistent way. This further model is expected to shed light on conditions where an electron avalanche can be engaged depending on both laser and material parameters.

ACKNOWLEDGMENT

Vladimir Tikhonchuk and Stefan Skupin are gratefully acknowledged for their comments regarding the present manuscript.

[1] S. Mironov, V. Lozhkarev, V. Ginzburg, and E. Khazanov, Appl. Opt. **48**, 2051 (2009).
[2] S. Mironov *et al.*, Quantum Electronics **41**, 963 (2011).
[3] M. Kolesik and J. Moloney, Rep. Prog. Phys. **77**, 016401 (2014).
[4] L. Berge, S. Skupin, R. Nuter, J. Kasparian, and J.-P. Wolf, Rep. Prog. Phys. **70**, 1633 (2007).
[5] A. Kaiser, B. Rethfeld, M. Vicanek, and G. Simon, Phys. Rev. B **61**, 11437 (2000).
[6] T. E. Itina, N. Shcheblanov, J.-P. Colombier, R. Stoian, E. Audouard, T. Y. Derrien, R. Torres, J. Hermann, M. E. Povarnitsyn, and K. V. Khishchenko, AIP Conf. Proc. **1278**, 38 (2010).
[7] J. R. Gulley, Proc. SPIE **7842**, 78420U (2010).
[8] J. R. Gulley and W. M. Dennis, Phys. Rev. A **81**, 033818 (2010).
[9] A. Bourgeade and G. Duchateau, Phys. Rev. E **85**, 056403 (2012).
[10] L. V. Keldysh, J. Exp. Theor. Phys. **33**, 994 (1957) [Sov. Phys. JETP **33**(6), 763 (1958)].
[11] J. Armstrong, N. Bloembergen, J. Ducuing, and P. Pershan, Phys. Rev. **127**, 1918 (1962).
[12] A. Bourgeade and E. Freysz, J. Opt. Soc. Am. B **17**, 226 (2000).
[13] A. Bourgeade and B. Nkonga, J. Supercomputing **28**, 279 (2004).
[14] C. Mezel, A. Bourgeade, and L. Hallo, Phys. Plasmas **17**, 113504 (2010).
[15] T. Brabec and F. Krausz, Phys. Rev. Lett. **78**, 3282 (1997).
[16] E. Louzon *et al.*, Appl. Phys. Lett. **87**, 241903 (2005).
[17] K. Yee, IEEE Trans. Antennas Propag. **AP-14**, 302 (1966).
[18] W. V. Houston, Phys. Rev. **57**, 184 (1940).
[19] J. Callaway, *Quantum Theory of the Solid State* (Academic, New York, 1974).
[20] J. R. Peñano, P. Sprangle, B. Hafizi, W. Manheimer, and A. Zigler, Phys. Rev. E **72**, 036412 (2005).
[21] P. Martin, S. Guizard, P. Daguzan, G. Petite, P. D'Oliveira, P. Meynadier, and M. Perdrix, Phys. Rev. B **55**, 5799 (1997).
[22] S. Guizard, P. D'Oliveira, P. Daguzan, P. Martin, P. Meynadier, and G. Petite, Nucl. Instrum. Methods B **116**, 43 (1996).
[23] F. Quere, S. Guizard, and P. Martin, Europhys. Lett. **56**, 138 (2001).
[24] G. Duchateau, G. Geoffroy, A. Dyan, H. Piombini, and S. Guizard, Phys. Rev. B **83**, 075114 (2011).
[25] L. Hallo, A. Bourgeade, V. T. Tikhonchuk, C. Mezel, and J. Breil, Phys. Rev. B **76**, 024101 (2007).
[26] E. G. Gamaly, S. Juodkazis, K. Nishimura, H. Misawa, B. Luther-Davies, L. Hallo, P. Nicolai, and V. T. Tikhonchuk, Phys. Rev. B **73**, 214101 (2006).
[27] M. B. Gaarde and A. Couairon, Phys. Rev. Lett. **103**, 043901 (2009).